

Ruelle-Pollicott Decay of Out-of-Time-Order Correlators in Many-Body Systems

Jerónimo Duarte,¹ Ignacio García-Mata,¹ and Diego A. Wisniacki²

¹*Instituto de Investigaciones Físicas de Mar del Plata (IFIMAR),
Facultad de Ciencias Exactas y Naturales, Universidad Nacional de Mar del Plata
& CONICET, Funes 3350 (7600) Mar del Plata, Argentina*

²*Departamento de Física “J. J. Giambiagi” and IFIBA, FCEyN,
Universidad de Buenos Aires, 1428 Buenos Aires, Argentina*

(Dated: October 22, 2025)

The out-of-time-order correlator (OTOC) quantifies information scrambling in quantum systems and serves as a key diagnostic of quantum chaos. In one-body systems with a classical counterpart, the relaxation of the OTOC is governed by Ruelle-Pollicott resonances. For many-body systems lacking a semiclassical limit, recent studies have identified an analogous role played by the Liouvillian spectrum of weakly open extensions of the dynamics, where the slowest decay rate – the Liouvillian gap – encodes relaxation. Here we study the kicked Ising spin chain and show that the long-time exponential decay of the OTOC in the isolated system occurs at a rate equal to twice this intrinsic gap. This correspondence persists even in crossover regimes between integrability and chaos, demonstrating that the Liouvillian spectrum provides a unified framework for understanding relaxation and irreversibility in closed many-body quantum systems.

I. INTRODUCTION

Understanding relaxation dynamics and the emergence of effective irreversibility in quantum many-body systems is a central problem at the interface of quantum chaos, statistical mechanics, and open-system theory. In classical chaotic dynamics, the intermediate time decay of correlations is governed by the Ruelle-Pollicott (RP) resonances [1–3] – isolated singularities of the analytically continued spectrum of the Frobenius-Perron operator – which generate effective irreversibility despite the underlying deterministic and reversible motion. In quantum one-body systems with a classical limit, an analogous correspondence is well established through spectral and operator-truncation approaches [4–6] or through weakly dissipative formulations [7–9].

In contrast, identifying the quantum analogue of RP resonances in generic many-body systems remains an open question. Several works [10–12] have introduced coarse-grained formulations of the operator space, revealing isolated eigenvalues inside the unit disk that can be interpreted as quantum RP resonances. While conceptually appealing, this approach becomes impractical for large systems due to the exponential growth of the operator space and the difficulty of defining an appropriate coarse-graining. A more recent development exploits translational invariance and quasi-momentum decomposition [13], enabling the identification of resonances within each symmetry sector.

An alternative line of research focuses on the Liouvillian spectrum of weakly open quantum systems [14]. When a system is coupled to an environment, its relaxation dynamics are governed by the eigenvalues of the corresponding Lindblad superoperator, with the slowest nonzero decay rate defining the Liouvillian gap. In exactly solvable models [15–17], this gap has been shown to coincide with the leading RP resonance of the corresponding isolated dynamics.

The magnitude of the leading RP resonance determines the approach to equilibrium of dynamical observables, including the out-of-time-order correlator (OTOC). The OTOC measures the spread of local perturbations and serves as a sensitive probe of information scrambling in quantum systems. Although the butterfly effect in quantum chaos is not universal [18], the relaxation of the OTOC at late times provides a robust signature of underlying dynamics. In one-body systems, the crossover from integrability to chaos can be characterized through the OTOC decay rate [19], a result that extends to systems with mixed classical dynamics [20].

Here we extend this connection to many-body systems. We study the kicked Ising spin chain, a paradigmatic model that exhibits both integrable and chaotic regimes depending on its parameters. Specifically, we analyze three complementary quantities: (i) the Liouvillian gap \bar{g} extracted from a weakly dissipative version of the model, (ii) standard chaos indicators from spectral statistics and eigenstate delocalization, and (iii) the intermediate time exponential decay rate α of the OTOC in the isolated chain. We show that $\alpha \approx 2\bar{g}$ even in transitional regimes between integrability and chaos, establishing the Liouvillian gap as a qualitative (and quantitative) measure of integrability in quantum many-body systems.

II. MANY-BODY SYSTEM: KICKED ISING SPIN CHAIN

To investigate the interplay between relaxation dynamics, quantum chaos, and dissipation, we consider the kicked Ising spin chain [21, 22], a paradigmatic model of many-body Floquet dynamics. This system is particularly well suited to our study because its parameters allow for a continuous interpolation between integrable and chaotic behavior.

The model is defined by the time-periodic Hamiltonian

$$\hat{H}(t) = \hat{H}_{\text{free}} + \hat{H}_{\text{kick}} \tau \sum_{n=-\infty}^{\infty} \delta(t - n\tau), \quad (1)$$

where the “free” and “kick” components take the form

$$\begin{cases} \hat{H}_{\text{free}} = -J \sum_{i=0}^{L-2} \hat{\sigma}_i^z \hat{\sigma}_{i+1}^z - h_z \sum_{i=0}^{L-1} \hat{\sigma}_i^z, \\ \hat{H}_{\text{kick}} = -h_x \sum_{i=0}^{L-1} \hat{\sigma}_i^x. \end{cases} \quad (2)$$

Here, $\hat{\sigma}_i^\alpha$ ($\alpha = x, z$) denote Pauli operators acting on site i , J is the nearest-neighbor coupling, and h_x, h_z are transverse and longitudinal magnetic fields, respectively. The dynamics is stroboscopic with period τ , and the evolution over one period is governed by the Floquet operator

$$\hat{U}_F = \hat{U}_{\text{free}} \hat{U}_{\text{kick}}, \quad (3)$$

where

$$\begin{cases} \hat{U}_{\text{free}} = \exp(-i\hat{H}_{\text{free}}\tau), \\ \hat{U}_{\text{kick}} = \exp(-i\hat{H}_{\text{kick}}\tau). \end{cases} \quad (4)$$

This Floquet representation conveniently describes both unitary and, when extended, weakly dissipative evolutions.

Throughout this work we set $J = h_z = \tau = 1$ and vary the transverse field h_x , which controls the degree of chaoticity. These values ensure nontrivial dynamics while reducing the parameter space to a single effective control variable. All simulations are performed for system sizes up to $L = 12$ spins.

To understand the structure of the spectrum, it is essential to discuss the symmetries present in the model. Since we work with a Floquet operator, the relevant spectrum consists of quasienergies. Throughout this study we impose open boundary conditions (OBC). The system possesses an external reflection symmetry \hat{R} , which acts as

$$\hat{R} |m_1, m_2, \dots, m_{L-2}, m_{L-1}\rangle = |m_{L-1}, m_{L-2}, \dots, m_2, m_1\rangle,$$

where $|m_1, m_2, \dots, m_{L-1}\rangle$ denotes a computational-basis state. Because $[\hat{U}_F, \hat{R}] = 0$, the Hilbert space decomposes into two invariant subspaces corresponding to the eigenvalues $+1$ and -1 of \hat{R} , which we refer to as the *even* and *odd* parity sectors. This symmetry decomposition allows us to analyze each sector independently, avoiding spectral mixing and enabling a cleaner identification of chaotic behavior and Liouvillian relaxation modes.

III. QUANTUM CHAOS DIAGNOSTICS

To characterize the degree of quantum chaos in the kicked Ising spin chain, we employ two complementary

diagnostics: spectral statistics and eigenstate delocalization. These indicators enable us to distinguish between integrable, chaotic, and intermediate regimes, providing essential context for interpreting the behavior of the OTOC and its connection to the Liouvillian gap.

A well-established signature of quantum chaos is the statistical distribution of level spacings [23]. Chaotic systems exhibit Wigner-Dyson distributions predicted by random matrix theory (RMT), with the specific ensemble—in our case, the Circular Orthogonal Ensemble (COE)—determined by the symmetries of the system [24]. In contrast, integrable systems display Poisson statistics reflecting the presence of extensive conserved quantities [25].

Rather than computing the full level-spacing distribution, we employ the ratio of adjacent spacings [26], which provides a practical and robust diagnostic. For the Floquet operator satisfying

$$\hat{U}_F |\psi_n\rangle = e^{i\varphi_n} |\psi_n\rangle, \quad n = 1, 2, \dots, D, \quad (5)$$

where φ_n are the quasienergies, $|\psi_n\rangle$ are the eigenstates, and D is the Hilbert space dimension, we compute

$$r_n = \frac{\min(\delta_n, \delta_{n-1})}{\max(\delta_n, \delta_{n-1})}, \quad \delta_n = \varphi_{n+1} - \varphi_n. \quad (6)$$

The mean value $\langle r \rangle$ exhibits two distinct limits: $\langle r \rangle_{\text{COE}} \approx 0.5307$ for COE statistics and $\langle r \rangle_P \approx 0.3863$ for Poisson statistics [27, 28]. To interpolate between these limits, we define the normalized parameter

$$\eta = \frac{\langle r \rangle - \langle r \rangle_P}{\langle r \rangle_{\text{COE}} - \langle r \rangle_P}, \quad (7)$$

which provides a continuous measure ranging from $\eta \rightarrow 0$ in the integrable regime to $\eta \rightarrow 1$ in the fully chaotic regime.

A complementary diagnostic is provided by eigenstate delocalization, quantified through the participation ratio (PR) [29]. Consider an eigenstate $|\psi_i\rangle$ expanded in a reference basis $\{|\phi_j\rangle\}_{j=0}^{D-1}$ as $|\psi_i\rangle = \sum_j a_{ij} |\phi_j\rangle$. The participation ratio is defined as

$$\xi_E(i) = \left[\sum_{j=0}^{D-1} |a_{ij}|^4 \right]^{-1}. \quad (8)$$

This quantity measures how extended an eigenstate is in the chosen basis. Small values indicate localization, while high values signal delocalization. For chaotic systems consistent with RMT, the coefficients $|a_{ij}|^2$ behave as independent random variables, leading to typical values $\xi_E^{\text{deloc}} \approx D/3$, where D is the Hilbert space dimension [30, 31]. In our numerical analysis, we compute the average of $\xi_E(i)$ over all eigenstates.

These spectral and eigenstate-based chaos indicators provide a quantitative map of the dynamical regime of the system. We analyze their behavior as a function

of the transverse field strength h_x , which controls the kick strength in the Floquet dynamics. To avoid spectral mixing between symmetry sectors, all analyses are performed within the even-parity subspace, ensuring a clearer characterization of the underlying dynamical behavior. This characterization serves as a reference for studying the Liouvillian gap and exploring potential connections between unitary and dissipative indicators of quantum chaos.

IV. OUT-OF-TIME-ORDER CORRELATOR

The out-of-time-order correlator (OTOC) quantifies the scrambling of quantum information and is defined as the thermal expectation value of the squared commutator between two operators evaluated at different times:

$$C(t) = \left\langle \left[\hat{W}(t), \hat{V} \right] \left[\hat{W}(t), \hat{V} \right]^\dagger \right\rangle, \quad (9)$$

where $\hat{W}(t)$ is the Heisenberg picture evolution of \hat{W} . Expectation values are taken over the infinite-temperature ensemble, $\langle \cdot \rangle = \text{Tr}(\cdot)/D$, with D the Hilbert-space dimension. This ensemble is appropriate for Floquet systems or Hamiltonians with bounded spectra, where microcanonical and infinite-temperature averages coincide in the thermodynamic limit.

Originally introduced in studies of superconductivity [32], the OTOC has become a central tool for characterizing quantum chaos and information scrambling in many-body systems [33]. The OTOC gained attention when upper bound for the exponential growth was found [34], setting the bar for fast scramblers like black holes[35] and strongly correlated fermionic systems[36–38]. In systems with a classical limit, the growth rate coincides with the classical Lyapunov exponent [19, 39–41]. At later times, quantum interference leads to saturation around a constant plateau with residual fluctuations that depend on the underlying dynamics [42].

We focus on local Hermitian and unitary operators \hat{W} and \hat{V} acting on distinct sites of the spin chain. A convenient choice is given by Pauli operators $\hat{\sigma}_i^\mu$ ($\mu = x, y, z$) acting on site i . At infinite temperature, the OTOC takes the explicit form

$$\begin{aligned} C^{\mu\nu}(l, t) &= \frac{1}{2} \left\langle [\hat{\sigma}_0^\mu(t), \hat{\sigma}_l^\nu]^2 \right\rangle \\ &= 1 - \frac{1}{D} \text{Re} \left\{ \text{Tr} [\hat{\sigma}_0^\mu(t) \hat{\sigma}_l^\nu \hat{\sigma}_0^\mu(t) \hat{\sigma}_l^\nu] \right\}. \end{aligned} \quad (10)$$

We define

$$O_1^{\mu\nu}(l, t) = \frac{1}{D} \text{Re} \left\{ \text{Tr} [\hat{\sigma}_0^\mu(t) \hat{\sigma}_l^\nu \hat{\sigma}_0^\mu(t) \hat{\sigma}_l^\nu] \right\}, \quad (11)$$

so that $C^{\mu\nu}(l, t) = 1 - O_1^{\mu\nu}(l, t)$. In what follows we focus on the case $\mu = \nu = z$, denoted $C^{zz}(l, t)$, which probes the scrambling and relaxation of local $\hat{\sigma}^z$ operators.

At intermediate times, the approach to saturation of $C(t)$, at (what we will call intermediate times) is reflected by an exponential decay of $O_1(t)$, which can be present even in systems which are not completely chaotic [20]. For one-body, completely chaotic systems, the decay is given by the classical RP resonances[19].

Figure 1 illustrates the time evolution of $|O_1^{zz}(l, t)|$ for $l = 1$ and a transverse field h_x deep in the chaotic regime. The data, obtained for $L = 12$, display a clear exponential decay at intermediate times. An exponential fit of the form $|O_1^{zz}(1, t)| \propto e^{-\alpha t}$ yields the decay rate α , which we compare below with twice the Liouvillian relaxation rate extracted from the weakly dissipative extension of the model.

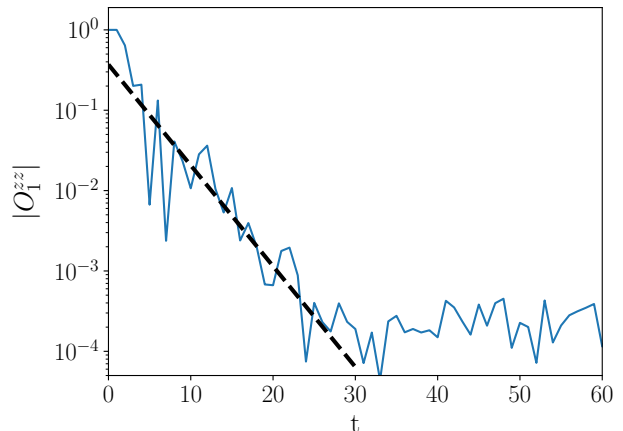


FIG. 1. The absolute value of $O_1^{zz}(1, t)$ for a transverse field h_x in the chaotic regime. The data corresponds to a spin chain of size $L = 12$ and $h_x = 0.8168$. The blue line with circles represents $O_1^{zz}(1, t)$, while the dashed line is the exponential fit to the intermediate time behavior of $|O_1^{zz}(1, t)|$, with a decay exponent $\alpha = 0.2888$.

V. LIOUVILLIAN GAP

To investigate the relation between the decay rate discussed in the previous section and the spectral properties of the system, we follow Ref. [14]. In this approach, the system is extended to a weakly open setting described by a Liouvillian superoperator

$$\mathcal{L} = -i[H, \cdot] + \gamma \mathcal{D}, \quad (12)$$

where \mathcal{D} is a dissipator and γ the dissipation strength. Building on the kicked Ising model defined above, we introduce bulk dephasing and study the corresponding relaxation dynamics through the time-periodic Lindblad master equation

$$\begin{aligned} \frac{d\rho}{dt} &= -i[\hat{H}(t), \rho] + \gamma \sum_{i=0}^{L-1} \left(\sigma_i^z \rho \sigma_i^z - \frac{1}{2} \{ \sigma_i^z \sigma_i^z, \rho \} \right) \\ &\equiv \mathcal{L}(t) \rho, \end{aligned} \quad (13)$$

where $\gamma > 0$ controls the dephasing strength and $\hat{H}(t) = \hat{H}(t + \tau)$ is the Floquet Hamiltonian.

The Liouvillian superoperator $\mathcal{L}(t)$ has a complex spectrum λ_α with negative real parts. For time-independent generators (\mathcal{L}) there is one zero mode ($\lambda_0 = 0$) corresponding to the steady state, plus decaying modes with $\text{Re } \lambda_\alpha < 0$. The Liouvillian gap

$$g = -\max_{\alpha \neq 0} \text{Re } \lambda_\alpha \quad (14)$$

characterizes the slowest non-trivial relaxation rate. In periodically driven systems it is convenient to define the Floquet map

$$\mathcal{U}_F = \mathcal{T} e^{\int_0^\tau \mathcal{L}(t) dt} \quad (15)$$

where \mathcal{T} denotes time ordering. The eigenvalues of \mathcal{U}_F are $e^{\lambda_\alpha \tau}$, allowing one to extract g equivalently from the Floquet-Liouvillian spectrum.

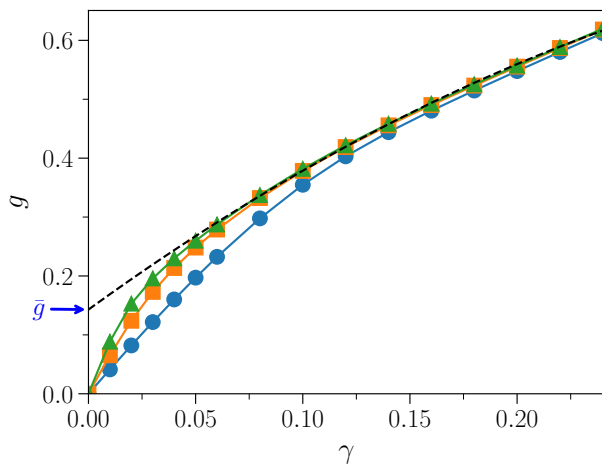


FIG. 2. Liouvillian gap $g(\gamma)$ as a function of the dissipation strength γ for system sizes $L = 6$ (blue circles), $L = 8$ (orange squares), and $L = 10$ (green triangles) and $h_x = 0.8168$. The dashed line indicate quadratic fit. For $L = 10$, the extrapolated value of \bar{g} is 0.1429

In chaotic many-body systems, it has been shown that taking the limits $L \rightarrow \infty$ first and $\gamma \rightarrow 0$, the gap converges to a nonzero limit

$$\bar{g} = \lim_{\gamma \rightarrow 0} \lim_{L \rightarrow \infty} g, \quad (16)$$

which coincides with the real part of the leading Ruelle-Pollicott resonance of the corresponding isolated chain [14].

To extract \bar{g} in the weak dissipation regime, we compute $g(\gamma)$ for several small values of γ and perform a quadratic fit in γ . Following Eq. (16), the fit is applied to the largest available system size. The eigenvalues of the Floquet-Liouvillian spectrum, from which $g(\gamma)$ is obtained, are computed using the Arnoldi-Lindblad method

described in Appendix A. This procedure provides the extrapolated value $\bar{g} \equiv \lim_{\gamma \rightarrow 0} \lim_{L \rightarrow \infty} g(\gamma)$, characterizing the intrinsic relaxation of the isolated chain.

Figure 2 shows the Liouvillian gap $g(\gamma)$ as a function of the dissipation strength for system sizes $L = 6, 8, 10$ at $h_x = 0.8168$. Dashed lines indicate quadratic fits, and for $L = 10$ the extrapolated value $\bar{g} = 0.1429$. Remarkably, the corresponding OTOC decay rate obtained in the isolated chain satisfies $\alpha \simeq 2\bar{g}$, demonstrating that the Liouvillian relaxation rate of the weakly open system predicts the intermediate time OTOC decay in the closed dynamics.

Parity-resolved analysis – We analyze the Liouvillian spectrum further within each parity subspace. Across the integrable-to-chaotic transition, the gaps of the two subspaces intersect when plotted as a function of the dissipation strength. As a result, the smallest nonzero eigenvalue – and hence the global Liouvillian gap – originates from the even subspace in certain parameter regions, while in others it comes from the odd subspace. This leads to an effective switching between sectors, so that the extracted global Liouvillian gap combines contributions from both subspaces depending on which hosts the slowest decaying mode. Importantly, this does not imply that the Arnoldi-Lindblad method is superior to the approach in Ref. [14]; rather, it allows us to probe parameter regimes – particularly the crossover from integrable to chaotic dynamics – where the behavior of the Liouvillian gaps can be resolved in detail.

To carry out this analysis, we explicitly constructed both the Lindbladian superoperator and the spatial inversion superoperator. By diagonalizing the latter, we obtained its eigenvalues and eigenvectors, which allowed us to separate the Hilbert space into parity-even and parity-odd subspaces. Since the Lindbladian commutes with the spatial inversion operator, it can be represented in this eigenbasis as a block-diagonal matrix, with one block corresponding to each parity sector. Restricting the dynamics to each block separately, we extracted the eigenvalues of the Lindbladian within each subspace, and thereby determined the corresponding parity-resolved Liouvillian gaps.

Figure 3 compares the Liouvillian gaps computed within each parity subspace – parity-even (blue empty circles) and parity-odd (orange empty squares) – with the global gap obtained via the Arnoldi-Lindblad method (green crosses). Solid lines serve as guides to the eye for the subspace gaps. As the dissipation parameter is varied, the dominant eigenvalue can switch between subspaces: in certain regions the even sector exhibits the smallest eigenvalue, while in others the odd sector becomes dominant. The Arnoldi method naturally captures this transition, since it always selects the eigenvalue with the smallest real part across all subspaces. Moreover, as the system size increases, the spectra of the two parity sectors become increasingly separated, making such crossings less probable. This behavior highlights that the Arnoldi approach consistently identifies the slowest

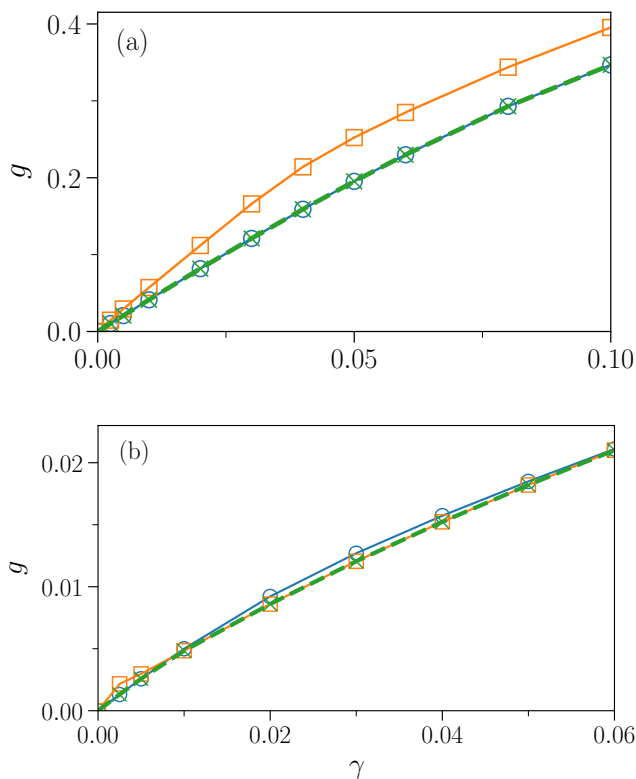


FIG. 3. Comparison of Liouvillian gaps for two values of the transverse field h_x . (a) $h_x = 0.7854$. The parity-even subspace is shown in blue empty circles, the parity-odd subspace in orange empty squares, and the global gap obtained via the Arnoldi-Lindblad method in green crosses. (b) $h_x = 0.2749$. The parity- even subspace is shown in blue empty circles, the parity- odd subspace in orange empty squares, and the global gap obtained via the Arnoldi-Lindblad method in green crosses.

decaying mode of the global dynamics, regardless of the underlying sectoral structure.

The case analyzed in Fig. 3(a) corresponds to the fully chaotic regime, where the Liouvillian gap curves for the two parity subspaces are clearly separated and no crossings occur, reflecting a well-defined hierarchy of decay rates between the sectors. In contrast, Fig. 3(b) shows an intermediate regime between integrability and chaos, where the curves partially overlap and crossings emerge, indicating that the slowest decaying mode can originate from either subspace depending on the dissipation strength. Both regimes are further illustrated in Fig. 4, highlighting how the Arnoldi-Lindblad method effectively captures the dominant relaxation dynamics and smoothly interpolates between different contributions as the system transitions from integrable to chaotic behavior.

VI. RELATION BETWEEN OTOC DECAY, THE LIOUVILLIAN GAP AND CHAOS PARAMETERS

In this section, we bring together the chaos indicators, OTOC decay exponents, and the Liouvillian gap – into a single comparative framework. Previously, we have shown how to compute the normalized level – spacing ratio η and participation ratio $\bar{\xi}_E$ across different transverse fields h_x , how to extract the intermediate time exponential decay exponent α of the local correlator $O_1^{zz}(l=1, t)$, and how to obtain the Liouvillian gap \bar{g} via quadratic extrapolation in the weak – dissipation limit for $L = 10$.

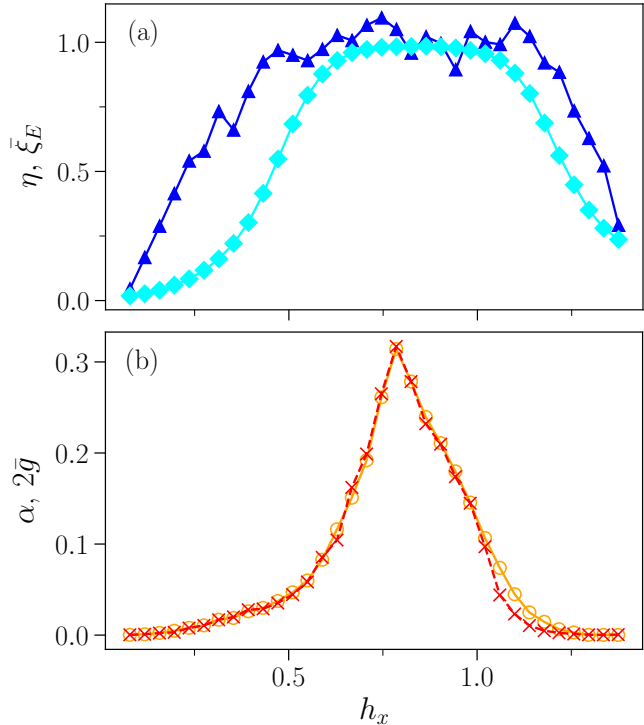


FIG. 4. (a) Chaos indicators η and $\bar{\xi}_E$ as functions of the transverse field h_x , computed from the Floquet spectrum in the parity-even subspace for system size $L = 12$. Blue upward triangles denote η and cyan diamonds denote $\bar{\xi}_E$. (b) Comparison between the OTOC decay exponent α (red crosses) and twice the Liouvillian gap $2\bar{g}$ (orange empty circles) as functions of h_x . The Liouvillian gap \bar{g} is extrapolated for $L = 10$, while α is obtained from the isolated chain with $L = 12$. The two panels together illustrate how both dynamical and spectral quantities capture the transition between integrable and chaotic regimes.

Figure 4(a) displays the chaos indicators η (blue upward triangles) and $\bar{\xi}_E$ (cyan diamonds) as functions of the transverse field h_x . Both quantities are computed from the unitary Floquet spectrum at system size $L = 12$, and – owing to the symmetries of the model – are analyzed within the parity-even subspace defined with respect to the external reflection operator. These indicators clearly capture the crossover from integrability to chaos.

Figure 4(b) shows the comparison between the OTOC decay exponent α (red crosses) and twice the Liouvillian gap $2\bar{g}$ (orange empty circles) as functions of h_x . For each value of h_x , α is obtained by fitting $|O_1^{zz}(1, t)|$ to an exponential decay at intermediate times in the isolated chain of size $L = 12$, while \bar{g} is extrapolated from $g(\gamma)$ for $L = 10$. The two quantities closely track each other across both fully chaotic and transitional regimes.

Overall, this figure highlights that the OTOC decay exponent remains approximately equal to twice the Liouvillian gap for all h_x values where scrambling-induced relaxation persists. For $h_x > 1.00$, the correspondence becomes less pronounced, likely due to finite-size effects – larger system sizes would be required to achieve quantitative convergence of both α and \bar{g} in this regime. Nevertheless, even at these modest sizes, a clear qualitative and quantitative agreement is observed, underscoring the robustness of the relationship between the OTOC decay rate and the Liouvillian gap.

It is worth noting that the decay exponent α and the Liouvillian gap \bar{g} qualitatively track the transition between dynamical regimes. A similar qualitative (and quantitative) behavior of the OTOC decay was previously reported for quantum maps in Ref. [20].

VII. CONCLUSIONS

We have investigated the connection between the decay of the out-of-time-order correlator (OTOC), the Liouvillian gap, and spectral indicators of chaos in many-body quantum systems, focusing on the kicked Ising spin chain. Our central finding is that the intermediate time exponential decay rate of the OTOC for generic, symmetry-unresolved operators equals twice the Liouvillian gap of the corresponding weakly open extension of the dynamics. This correspondence, previously established for systems with a semiclassical limit, is shown here to persist across the entire crossover from integrable to chaotic regimes, demonstrating that the Liouvillian spectrum provides a unifying description of relaxation and irreversibility in quantum many-body dynamics.

A detailed parity-resolved analysis confirms that the intrinsic Liouvillian gap extracted from the Arnoldi-Lindblad method reproduces the global relaxation rate of the system, even when the dominant decay mode shifts between symmetry sectors. This robustness highlights that both the OTOC and the Liouvillian gap respond coherently to changes in the underlying dynamical regime, providing consistent signatures of the transition from integrability to chaos.

The practicality of the Arnoldi-Lindblad approach lies in its ability to access the smallest Liouvillian eigenvalues without constructing the full superoperator, enabling efficient computation of the Liouvillian gap and its extrapolation to the weak-dissipation limit. In contrast to the momentum-resolved analysis of Ref. [13] for systems with periodic boundary conditions, our framework cap-

tures the global relaxation properties of the chain under open boundaries, providing a complementary perspective that links spectral relaxation modes directly to information scrambling.

Overall, our results establish a quantitative bridge between unitary and dissipative descriptions of quantum relaxation, extending the Liouvillian-OTOC correspondence beyond the fully chaotic regime. This connection suggests that Liouvillian spectroscopy may serve as a general diagnostic tool for intermediate time dynamics and operator spreading in isolated quantum systems.

ACKNOWLEDGMENTS

We acknowledge support from Argentinian Agencia I+D+i (Grants No. PICT-2020-SERIEA-00740 and PICT-2020-SERIEA-01082). I.G-M received support from the French-Argentinian International Research Project *Complex Quantum Systems* (COQSYS), funded by CNRS. D.A.W. received support from CONICET (Grant No. PIP 11220200100568CO), UBACyT (Grant No. 20020220300049BA) and PREI-UNAM.

Appendix A: Arnoldi-Lindblad time evolution

To compute the Liouvillian spectrum efficiently, we employ the *Arnoldi-Lindblad approach* of Ref. [43]. This method allows one to access the smallest-magnitude eigenvalues of the Floquet-Lindbladian without constructing the full superoperator, whose matrix representation has dimensions $D^2 \times D^2$, with D being the Hilbert-space dimension. As a result, explicitly building the Liouvillian quickly becomes computationally prohibitive as the system size increases.

We consider a periodically driven open quantum system whose stroboscopic dynamics is governed by the Lindblad master equation of period T ,

$$\partial_t \hat{\rho}(t) = \mathcal{L}(t) \hat{\rho}(t), \quad \mathcal{L}(t) = \mathcal{L}(t + T). \quad (\text{A1})$$

The evolution over one period is formally given by the time-ordered exponential

$$\hat{\rho}(T) = \mathcal{T} \left[\exp \left(\int_0^T \mathcal{L}(t') dt' \right) \right] \hat{\rho}(0) \equiv \mathcal{F}(T, 0) \hat{\rho}(0), \quad (\text{A2})$$

where $\mathcal{F}(T, 0)$ denotes the *Floquet map* associated with one full period of evolution.

By periodicity,

$$\mathcal{F}(t, 0) = [\mathcal{F}(T, 0)]^n \mathcal{F}(t - nT, 0), \quad (\text{A3})$$

for integer n . Defining the Floquet Liouvillian \mathcal{L}_F through

$$\mathcal{F}(T, 0) = \exp(\mathcal{L}_F T), \quad (\text{A4})$$

one obtains

$$\mathcal{F} \hat{\rho}_j^F = \varphi_j^F \hat{\rho}_j^F = e^{\lambda_j^F T} \hat{\rho}_j^F \iff \mathcal{L}_F \hat{\rho}_j^F = \lambda_j^F \hat{\rho}_j^F. \quad (\text{A5})$$

The eigenvalues λ_j^F form the Floquet-Liouvillian spectrum, from which the Liouvillian gap $g = -\max_{\alpha \neq 0} \text{Re } \lambda_\alpha^F$ is extracted.

In practice, we generate the Krylov subspace

$$\begin{aligned} \mathcal{K}_n &= \{\hat{\rho}(0), \hat{\rho}(T), \hat{\rho}(2T), \dots, \hat{\rho}(nT)\} \\ &= \{\hat{\rho}(0), \mathcal{F}\hat{\rho}(0), \mathcal{F}^2\hat{\rho}(0), \dots, \mathcal{F}^n\hat{\rho}(0)\}. \end{aligned} \quad (\text{A6})$$

directly from time evolution under the Lindblad equation, without explicitly constructing \mathcal{L} or \mathcal{F} . Applying the Arnoldi iteration to this subspace yields an effective

Hessenberg matrix whose eigenvalues approximate those of \mathcal{F} , providing the leading relaxation rates of the Liouvillian spectrum. The key advantage of this method is that the resulting Hessenberg matrix has dimensions $n \times n$, with $n \ll D^2$, thus drastically reducing the computational cost compared to handling the full Liouvillian superoperator.

We validated the implementation by explicitly constructing \mathcal{L} for small system sizes ($L = 4, 5, 6$) and comparing the resulting eigenvalues with those obtained from the Arnoldi-Lindblad method. The agreement was excellent, confirming the accuracy and efficiency of the approach.

-
- [1] D. Ruelle, Locating resonances for axiom a dynamical systems, *J. Stat. Phys.* **44**, 281 (1986).
- [2] D. Ruelle, Resonances of chaotic dynamical systems, *Phys. Rev. Lett.* **56**, 405 (1986).
- [3] M. Pollicott, On the rate of mixing of axiom a flows, *Inventiones mathematicae* **81**, 413 (1985).
- [4] C. Manderfeld, J. Weber, and F. Haake, Classical versus quantum time evolution of (quasi-) probability densities at limited phase-space resolution, *J. Phys. A: Math. Gen.* **34**, 9893 (2001).
- [5] M. Khodas and S. Fishman, Relaxation and diffusion for the kicked rotor, *Phys. Rev. Lett.* **84**, 2837 (2000).
- [6] S. Fishman and S. Rahav, Relaxation and noise in chaotic systems, in *Dynamics of Dissipation*, edited by P. Garbaczewski and R. Olkiewicz (Springer Berlin Heidelberg, Berlin, Heidelberg, 2002) pp. 165–192.
- [7] S. Nonnenmacher, Spectral properties of noisy classical and quantum propagators, *Nonlinearity* **16**, 1685 (2003).
- [8] I. García-Mata and M. Saraceno, Spectral properties and classical decays in quantum open systems, *Physical Review E* **69**, 056211 (2004).
- [9] I. García-Mata and M. Saraceno, Spectral approach to chaos and quantum-classical correspondence in quantum maps, *Mod. Phys. Lett. B* **19**, 341 (2005).
- [10] T. Prosen, Ruelle resonances in quantum many-body dynamics, *J. Phys. A: Math. & Gen* **35**, L737 (2002).
- [11] T. Prosen, Ruelle resonances in kicked quantum spin chain, *Physica D* **187**, 244 (2004).
- [12] T. Prosen, Chaos and complexity of quantum motion, *J. Phys. A: Math. & Gen.* **40**, 7881 (2007).
- [13] M. Žnidarič, Momentum-dependent quantum ruelle-pollicott resonances in translationally invariant many-body systems, *Phys. Rev. E* **110**, 054204 (2024) (2024).
- [14] T. Mori, Liouvillian-gap analysis of open quantum many-body systems in the weak dissipation limit, *Physical Review B* **109**, 064311 (2024).
- [15] J. A. Jacoby, D. A. Huse, and S. Gopalakrishnan, Spectral gaps of local quantum channels in the weak-dissipation limit, *Phys. Rev. B* **111**, 104303 (2025).
- [16] C. Zhang, L. Nie, and C. von Keyserlingk, Thermalization rates and quantum ruelle-pollicott resonances: insights from operator hydrodynamics, arXiv preprint arXiv:2409.17251 (2024).
- [17] T. Yoshimura and L. Sá, Theory of irreversibility in quantum many-body systems, *Phys. Rev. E* **111**, 064135 (2025).
- [18] I. García-Mata, R. A. Jalabert, and D. A. Wisniacki, Out-of-time-order correlations and quantum chaos, *Scholarpedia* **18**, 55237 (2023).
- [19] I. García-Mata, M. Saraceno, R. A. Jalabert, A. J. Roncaglia, and D. A. Wisniacki, Chaos signatures in the short and long time behavior of the out-of-time ordered correlator, *Phys. Rev. Lett.* **121**, 210601 (2018).
- [20] T. Notenson, I. García-Mata, A. J. Roncaglia, and D. A. Wisniacki, Classical approach to equilibrium of out-of-time ordered correlators in mixed systems, *Phys. Rev. E* **107**, 064207 (2023).
- [21] T. Prosen, Exact time-correlation functions of quantum ising chain in a kicking transversal magnetic field: Spectral analysis of the adjoint propagator in heisenberg picture, *Prog. Theor. Phys. Suppl.* **139**, 191 (2000).
- [22] T. Prosen, General relation between quantum ergodicity and fidelity of quantum dynamics, *Phys. Rev. E* **65**, 036208 (2002).
- [23] O. Bohigas, M. J. Giannoni, and C. Schmit, Characterization of chaotic quantum spectra and universality of level fluctuation laws, *Phys. Rev. Lett.* **52**, 1 (1984).
- [24] M. L. Mehta, *Random matrices*, Vol. 142 (Elsevier, 2004).
- [25] M. V. Berry and M. Tabor, Level clustering in the regular spectrum, *Proceedings of the Royal Society of London. A. Mathematical and Physical Sciences* **356**, 375 (1977).
- [26] V. Oganesyan and D. A. Huse, Localization of interacting fermions at high temperature, *Phys. Rev. B* **75**, 155111 (2007).
- [27] Y. Y. Atas, E. Bogomolny, O. Giraud, and G. Roux, Distribution of the ratio of consecutive level spacings in random matrix ensembles, *Phys. Rev. Lett.* **110**, 084101 (2013).
- [28] P. A. Lee and T. V. Ramakrishnan, Disordered electronic systems, *Rev. Mod. Phys.* **57**, 287 (1985).
- [29] F. Wegner, Inverse participation ratio in $2 + \varepsilon$ dimensions, *Zeitschrift für Physik B Condensed Matter* **36**, 209 (1980).
- [30] A. Gubin and L. F. Santos, Quantum chaos: An introduction via chains of interacting spins 1/2, *Am. J. Phys.* **80**, 246 (2012).

- [31] V. Zelevinsky, B. A. Brown, N. Frazier, and M. Horoi, The nuclear shell model as a testing ground for many-body quantum chaos, *Physics Reports* **276**, 85 (1996).
- [32] A. Larkin and Y. N. Ovchinnikov, Quasiclassical method in the theory of superconductivity, *Sov Phys JETP* **28**, 1200 (1969).
- [33] S. Xu and B. Swingle, Scrambling dynamics and out-of-time-ordered correlators in quantum many-body systems, *PRX Quantum* **5**, 010201 (2024).
- [34] J. Maldacena, S. H. Shenker, and D. Stanford, A bound on chaos, *Journal of High Energy Physics* **2016**, 1 (2016).
- [35] S. H. Shenker and D. Stanford, Black holes and the butterfly effect, *Journal of High Energy Physics* **2014** (2013).
- [36] S. Sachdev and J. Ye, Gapless spin-fluid ground state in a random quantum heisenberg magnet, *Phys. Rev. Lett.* **70**, 3339 (1993).
- [37] A. Kitaev, *A simple model of quantum holography, talk given at KITP Program: Entanglement in Strongly-Correlated Quantum Matter*, Vol. 7 (USA April, 2015).
- [38] J. Maldacena and D. Stanford, Remarks on the Sachdev-Ye-Kitaev model, *Phys. Rev. D* **94**, 106002 (2016).
- [39] E. B. Rozenbaum, S. Ganeshan, and V. Galitski, Lyapunov exponent and out-of-time-ordered correlator's growth rate in a chaotic system, *Phys. Rev. Lett.* **118**, 086801 (2017).
- [40] R. A. Jalabert, I. García-Mata, and D. A. Wisniacki, Semiclassical theory of out-of-time-order correlators for low-dimensional classically chaotic systems, *Phys. Rev. E* **98**, 062218 (2018).
- [41] X. Chen and T. Zhou, Operator scrambling and quantum chaos (2018).
- [42] E. M. Fortes, I. García-Mata, R. A. Jalabert, and D. A. Wisniacki, Gauging classical and quantum integrability through out-of-time-ordered correlators, *Phys. Rev. E* **100**, 042201 (2019).
- [43] F. Minganti and D. Huybrechts, Arnoldi-Lindblad time evolution: Faster-than-the-clock algorithm for the spectrum of time-independent and Floquet open quantum systems, *Quantum* **6**, 649 (2022).